PHYSICAL REVIEW D VOLUME 44, NUMBER 7 1 OCTOBER 1991

Four-heavy-quark hadroproduction

V. Barger and A. L. Stange
Physics Department, University of Wisconsin, Madison, Wisconsin 53706

R. J. N. Phillips
Rutherford Appleton Laboratory, Chilton, Didcot, Oxon, England
(Received 26 February 1991; revised manuscript received 25 June 1991)

We present new formulas for the numerical calculation of QCD production of two pairs of heavy quarks in hadron collisions, in leading order. We give results for $b\bar{b}b\bar{b}$, $b\bar{b}c\bar{c}$, and $c\bar{c}c\bar{c}$ production at the Fermilab Tevatron; the cross sections exceed 100 pb with all heavy quarks having $p_T > 10$ GeV. We also present results for $t\bar{t}t\bar{t}$ production in pp collisions for supercollider energies and briefly discuss the physics consequences for multi-W production via standard $t \to bW$ decays. For $m_t = 110$–140 GeV we predict of order 10–30 four-W events per year at the Superconducting Super Collider from this source, with all four weak bosons decaying to $e\nu_e$ or $\mu\nu_\mu$. Similar results are obtained for the CERN Large Hadron Collider, assuming ten times higher luminosity.

I. INTRODUCTION

The production of heavy quark flavors is of great interest at present and future hadron colliders. Topics of major physics interest in this connection are the discovery of the top quark t, the measurement of its mass m_t, the study of t decays, the study of B-meson decays including CP violation and loop-mediated rare decays, the measurement of B_s-$\bar{B}_s$ mixing, and the heavy-flavor content of jets. The dominant QCD process is pair production by $q\bar{q}$ or gg fusion. Multiple heavy quark production is also possible, however, via higher-order QCD processes. In the present paper we describe a new numerical method for calculating the hadroproduction of four heavy quarks, present cross section results for a number of important cases, and discuss some physics implications.

For higher-order QCD processes, the calculation of color factors and spin-dependent matrix elements is complicated. Our approach, described in Sec. II, is based on a direct numerical computation of color factors coupled with a direct computation of Dirac spinor products.

In Sec. III we present a selection of results. For the $p\bar{p}$ Tevatron collider, at c.m. energy $\sqrt{s} = 1.8$ TeV, we give cross sections and some dynamical distributions for the production of $b\bar{b}b\bar{b}$, $b\bar{b}c\bar{c}$, and $c\bar{c}c\bar{c}$ heavy quark combinations. The cross sections exceed 100 pb with all heavy quarks having $p_T > 10$ GeV. These channels in principle offer fresh tests of QCD; they are also interesting as major sources of multilepton events, via b and c semileptonic decays. For supercolliders we give the $pp \to t\bar{t}t\bar{t}X$ cross section as a function of energy for various m_t values, and present some cross sections and dynamical distributions at $\sqrt{s} = 40$ TeV, the energy of the Superconducting Super Collider (SSC). We discuss some physical implications of the four-top-quark production mechanism; in particular, it leads to $W^+W^+W^-W^-$ events via the standard $t \to bW$ decay mechanism. We give the cross sections for various multi-W decay configurations at $\sqrt{s} = 15.4$ and 40 TeV, corresponding to the CERN Large Hadron Collider (LHC) and the SSC. We predict of order 10–30 events with all four W bosons decaying to $e\nu_e$ and $\mu\nu_\mu$, for top quark masses of order 110–140 GeV and nominal annual luminosity $\mathcal{L} = 10$ fb^{-1} at the SSC; similar event rates are found for the LHC, assuming ten times higher luminosity.

II. METHODS OF CALCULATION

The leading QCD subprocesses for the production of two pairs of heavy quarks $Q_2\bar{Q}_2$ and $Q_3\bar{Q}_3$ (initially assumed to have different flavors) are light-quark–antiquark fusion and gluon-gluon fusion:

$$q_1^i + \bar{q}_1^j \to Q_2^k + \bar{Q}_2^l + Q_3^m + \bar{Q}_3^n \,, \tag{1}$$

$$g^a + g^b \to Q_2^k + \bar{Q}_2^l + Q_3^m + \bar{Q}_3^n \,, \tag{2}$$

where the subscripts $1,2,3$ denote quark flavors and superscripts $i,j,k,l,m,n = 1,2,3$ and $a,b = 1,\ldots,8$ label the color states.

We first consider in detail the case of gluon-gluon fusion, Eq. (2). There are 36 contributing Feynman diagrams, representative examples of which are shown in Fig. 1. However, due to the four-gluon interaction in Fig. 1(c), which has three independent color structures, there are 38 distinct amplitudes contributing to the matrix element. We discuss this process as if there were 38 Feynman diagrams.

The matrix element has the form

$$\mathcal{M}(a,b,k,l,m,n) = \sum_{\alpha=1}^{38} C_\alpha \mathcal{M}_\alpha, \tag{3}$$

where the subscript $\alpha = 1,2,\ldots,38$ refers to the corresponding Feynman diagram. Here C_α is a color factor and $\mathcal{M}_\alpha$ is the corresponding spin-dependent part of the

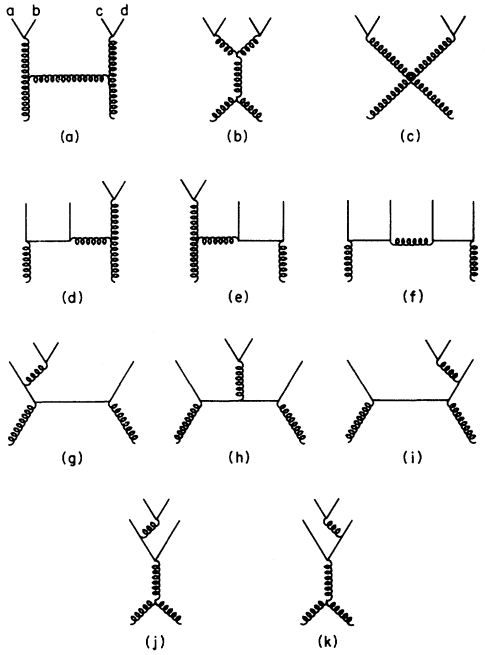

FIG. 1. Typical Feynman diagrams for the gluon fusion subprocess.

amplitude; the $\mathcal{M}_\alpha$ are given in Appendix A. The matrix element squared and summed over external colors then has the form

$$\sum_{\{\sigma\}} |\mathcal{M}|^2 = \mathcal{M}^*_\alpha \mathcal{C}_{\alpha\beta} \mathcal{M}_\beta \ , \tag{4}$$

where $\{\sigma\}$ denotes the set of external color indices $\{a,b,k,l,m,n\}$ and $\mathcal{C}_{\alpha\beta} = \sum_{\{\sigma\}} C^*_\alpha C_\beta$. As described in Ref. [1], the matrix elements $\mathcal{C}_{\alpha\beta}$ are evaluated numerically by creating a library of arrays $T(a,i,j) = T^a_{ij}$ for the Gell-Mann matrices and $f(a,b,c) = if^{abc}$ for the SU(3) structure constants, from which all necessary products and summations are constructed by successive simple instructions. The color matrix $\mathcal{C}_{\alpha\beta}$ is also presented in Appendix A.

We have compared our color matrix with the results obtained by the method of Gunion and Kunszt [2]; after correcting for an omission in rows 29 to 32 and color structures 3 through 6 in Table 2 in the first paper of Ref. [2], their results become consistent with ours.

The Feynman diagrams for the quark-antiquark fusion subprocess are shown in Fig. 2. The matrix element here has a similar form,

$$\mathcal{M}(i,j,k,l,m,n) = \sum_{\alpha=1}^{7} C_\alpha \mathcal{M}_\alpha \ , \tag{5}$$

where the subscript $\alpha = 1,2,\ldots,7$ labels the corresponding diagrams as before. The color matrix $\mathcal{C}_{\alpha\beta}$ and the invariant amplitudes $\mathcal{M}_\alpha$ for these subprocesses are given in Appendix B.

The amplitudes $\mathcal{M}_\alpha$ are computed numerically from

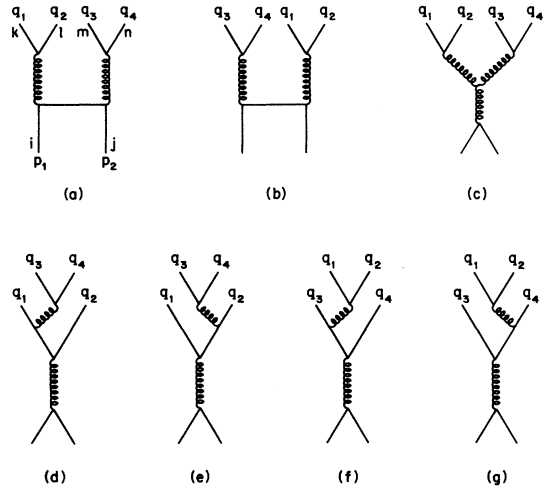

FIG. 2. Feynman diagrams for the quark-antiquark fusion subprocess.

products of four-component Dirac spinors, rather than the two-component spinors that are used in helicity amplitude evaluations for processes involving massless quarks [3].

A tree-level amplitude can be expressed in terms of fermion strings of the form

$$\bar{\psi}_2(p_2,\sigma_2)\, \not{a}_1\, \not{a}_2 \cdots \not{a}_n \psi_1(p_1,\sigma_1) \ , \tag{6}$$

where ψ_1, ψ_2 [$= u(p,\sigma)$ or $v(p,\sigma)$] are Dirac spinors, p and σ label the fermion four-momenta and helicities ($\sigma = \pm 1$) and $\not{a}_i = a_i^\mu \gamma_\mu$. The $\not{a}_i$ may be formed from particle four-momenta, gauge boson polarization vectors, fermion strings with an uncontracted Lorentz index or gauge boson couplings of the form $\gamma^\mu(g_V + g_A\gamma_5)$.

We use the chiral representation where the γ matrices are expressed in terms of 2×2 Pauli matrices $\boldsymbol{\sigma}$ and the unit matrix $\mathbf{1}$ as

$$\gamma^\mu = \begin{pmatrix} 0 & \sigma_+^\mu \\ \sigma_-^\mu & 0 \end{pmatrix}, \quad \gamma^5 = \begin{pmatrix} -\mathbf{1} & 0 \\ 0 & \mathbf{1} \end{pmatrix},$$
$$\sigma_\pm^\mu = (\mathbf{1}, \pm\boldsymbol{\sigma}), \tag{7}$$

giving

$$\not{a} = \begin{pmatrix} 0 & (\not{a})_+ \\ (\not{a})_- & 0 \end{pmatrix}, \quad (\not{a})_\pm = a_\mu \sigma_\pm^\mu \ . \tag{8}$$

The Dirac spinors are expressed in terms of two-component Weyl spinors $\psi_\pm$ as

$$\psi = \begin{pmatrix} \psi_- \\ \psi_+ \end{pmatrix}, \quad \psi = \left(\psi_+^\dagger \, , \, \psi_-^\dagger\right) \ . \tag{9}$$

The Weyl spinors are given in terms of helicity eigenstates $\chi_\lambda(p)$ with $\lambda = \pm 1$ by

$$u(p,\lambda)_\pm = (E \pm \lambda|\mathbf{p}|)^{1/2} \chi_\lambda(p) \ ,$$
$$v(p,\lambda)_\pm = \pm\lambda\,(E \mp \lambda|\mathbf{p}|)^{1/2} \chi_{-\lambda}(p) \ , \tag{10}$$

where $E = (|\mathbf{p}|^2 + m^2)^{1/2}$ and

$$\chi_+(p) = [2|\mathbf{p}|(|\mathbf{p}| + p_z)]^{-1/2} \begin{pmatrix} |\mathbf{p}| + p_z \\ p_x + ip_y \end{pmatrix}, \quad (11)$$

$$\chi_-(p) = [2|\mathbf{p}|(|\mathbf{p}| + p_z)]^{-1/2} \begin{pmatrix} -p_x + ip_y \\ |\mathbf{p}| + p_z \end{pmatrix}, \quad (12)$$

are the normalized helicity eigenspinors. For $p_z = -|\mathbf{p}|$ we follow the convention

$$\chi_+ = \begin{pmatrix} 0 \\ 1 \end{pmatrix}, \quad \chi_- = \begin{pmatrix} -1 \\ 0 \end{pmatrix}. \quad (13)$$

The gauge-boson polarization vectors $\epsilon^\mu(q,\alpha)$ are expressed in terms of the boson four-momenta as

$$\begin{aligned} \epsilon^\mu(q,\alpha=1) &= (|\mathbf{q}|q_T)^{-1}(0, q_x q_z, q_y q_z, -q_T^2), \\ \epsilon^\mu(q,\alpha=2) &= q_T^{-1}(0, -q_y, q_z, 0), \\ \epsilon^\mu(q,\alpha=3) &= [E_V/(M_V|\mathbf{q}|)](|\mathbf{q}|^2/E_V, q_x, q_y, q_z), \end{aligned} \quad (14)$$

and $q_T = (q_x^2 + q_y^2)^{1/2}$, $E_V = (|\mathbf{q}|^2 + M_V^2)^{1/2}$.

The usual crossing relations are maintained in the above formalism. It is possible to write down generic amplitudes and then apply crossing relations to particle momenta to obtain the amplitude for the desired process. To calculate $u(p,\sigma)$ where $p^0 < 0$, the identity $u(-p,\sigma) = v(p,-\sigma)$ is used. Here σ is the helicity for fermions and its negative for antifermions.

We find the above four-component amplitude method superior to extensions of the two-component formalism for the case of massive fermions in which we are interested. Implementation in FORTRAN programs is simple and straightforward, resulting in programs which are easy to read and debug. We have found that the resulting routines execute fairly quickly.

To check our computer codes we have performed a Lorentz invariance check on the squared amplitude summed over spin and color. We also performed a gauge invariance check at the amplitude level. This involves forming linearly independent combinations of the amplitudes, as determined by the eigenvectors of the color matrix given in Appendix A, and checking that they are invariant under the transformation $\epsilon^\mu(p) \to \epsilon^\mu(p) + p^\mu$. For the gluon fusion case with nonidentical quarks there are eleven nonzero eigenvalues providing eleven independent gauge invariance tests. For the quark-antiquark fusion case there are four nonzero eigenvalues and eigenvectors, but there is no external gluon and hence no gauge invariance check in this case.

Thus far we have assumed that the quark pairs have nonidentical flavors. However, both the color matrix calculation and the amplitude calculation are easily extended to handle the identical flavor calculation. In the gg fusion case there are 36 additional Feynman diagrams (contributing 38 more amplitudes, due to the four-gluon interaction); they can be obtained from the original set of diagrams by permuting the momentum, spin, and color of either the quark pair Q_2Q_3 or the antiquark pair $\bar{Q}_2\bar{Q}_3$ and reversing the signs of the additional amplitudes. Thus we have altogether 76 topologically distinct amplitudes $\mathcal{M}^\alpha$ for gg fusion to give identical quark pairs. In this case we also perform Lorentz invariance and gauge invariance checks. For the gluon-gluon fusion case there are twelve nonzero eigenvalues providing twelve independent gauge invariance checks. In the production of identical quark pairs by $q\bar{q}$ fusion, the original set of seven diagrams is doubled to 14 amplitudes.

After squaring the amplitudes we integrate both the identical-particle pairs Q_2Q_3 and $\bar{Q}_2\bar{Q}_3$ over all of phase space, dividing by $(2!)^2$ to avoid double counting in the total cross section.

III. RESULTS

In $p\bar{p}$ collisions at the Fermilab Tevatron collider, there is physics interest [4] in $b\bar{b}b\bar{b}$, $b\bar{b}c\bar{c}$, and $c\bar{c}c\bar{c}$ production, both as fresh testing-grounds for QCD and as sources of multilepton events via b or c semileptonic decays. Table I lists the integrated cross sections for these channels at $\sqrt{s} = 1.8$ TeV and also the cross sections for the cases that all four produced heavy quarks have transverse momenta $p_T > 5$ GeV and $p_T > 10$ GeV (so that the resulting jets and decay leptons may have high p_T). Here we have used $m_b = 5$ GeV and $m_c = 1.5$ GeV. The dependence on quark mass is reduced when high p_T is required, as generally expected. These and all subsequent results shown in the paper are calculated with the HMRSB parton distributions [5] evaluated at the scale $Q^2 = \hat{s}/4$ where $\hat{s}$ is the subprocess c.m. energy squared; the running coupling α_s is calculated at two-loop order. Figure 3 shows the distributions versus the invariant mass of the four produced quarks; although they peak strongly at threshold, there are substantial tails stretching out to very high invariant mass values, where multijet events may be expected. Figure 4 shows the cross sections for $b\bar{b}b\bar{b}$ events where 1, 2, 3, or 4 b quarks have transverse momenta $p_T(b) > p_T(\text{cut})$, versus $p_T(\text{cut})$. This is of direct experimental interest because events with several high-p_T b quarks are potentially identifiable via b-jet structure or b-decay leptons or microvertex criteria.

At SSC energies we expect the production of four b and/or c quarks to receive significant additional contributions from higher-order processes, such as gluon fragmentation in multi-jet events (our calculations only include $g \to b\bar{b}$ fragmentation in two-jet cases). The lowest-order cross section will therefore provide simply a lower bound on the total production of four such quarks; for $b\bar{b}b\bar{b}$ production we calculate the lowest-order contribution to be 0.29 μb at $\sqrt{s} = 40$ TeV [to be compared with $\mathcal{O}(\alpha_s^3)$ $b\bar{b}$ two-quark production of order 280 μb at the scale $Q = m_b$].

TABLE I. Four-quark production cross sections in nb at the Tevatron.

Source	Cross section (nb)		
	$p_T > 0$ GeV	$p_T > 5$ GeV	$p_T > 10$ GeV
$b\bar{b}b\bar{b}$	3.3	0.82	0.12
$b\bar{b}c\bar{c}$	68	4.2	0.27
$c\bar{c}c\bar{c}$	490	6.8	0.44

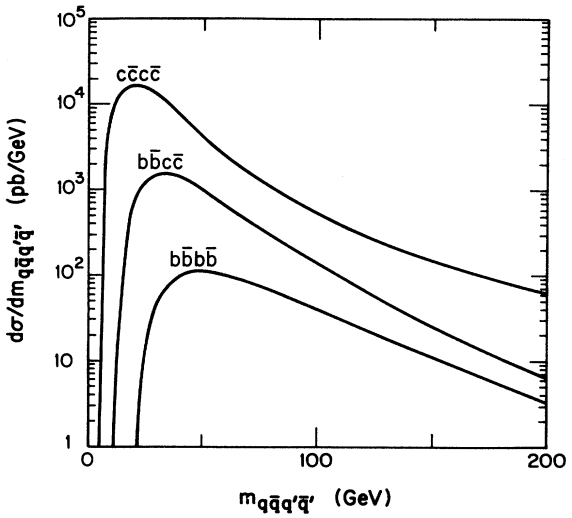

FIG. 3. Distributions versus the invariant mass of the four heavy quarks produced in $p\bar{p} \to b\bar{b}b\bar{b}$, $b\bar{b}c\bar{c}$, and $c\bar{c}c\bar{c}$ channels at the Tevatron energy, $\sqrt{s} = 1.8$ TeV.

The principal interest of our calculations at supercollider energies is therefore in the $t\bar{t}t\bar{t}$ channel. We concentrate attention here on the mass range above the Collider Detector at Fermilab experimental lower limit [6] $m_t > 89$ GeV and below the theoretical upper limit $m_t \lesssim 200$ GeV indicated by the analysis of radiative corrections [7] within the standard model. There are no previous calculations in this important mass range. Our results for smaller quark masses are within a factor of 2 of previous calculations [8] when we use the same sets of structure functions; the color matrix discrepancy noted earlier may account for this difference.

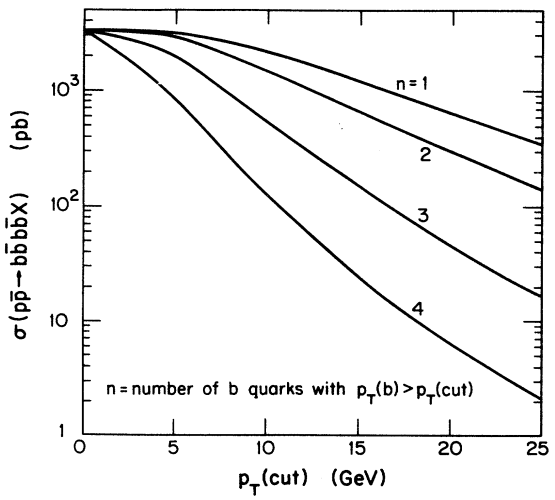

FIG. 4. Cross sections for $p\bar{p} \to b\bar{b}b\bar{b}$ production where 1, 2, 3, or 4 b quarks have transverse momenta $p_T(b) > p_T(\text{cut})$, versus $p_T(\text{cut})$, at $\sqrt{s} = 1.8$ TeV.

Figure 5 shows the integrated cross section $\sigma(pp \to t\bar{t}t\bar{t}X)$ for the production of four top quarks versus the pp c.m. energy $\sqrt{s}$, for the cases $m_t = 110$, 140, 170, 200 GeV. Arrows indicate the energies $\sqrt{s} = 15.4$ and 40 TeV of the LHC and SSC supercolliders. For comparison, the cross section $\sigma(pp \to t\bar{t}X)$ for the production of two top quarks is also shown, scaled down by a factor of 10^{-3}, for $m_t = 140$ GeV; it was calculated here to $\mathcal{O}(\alpha_s^3)$ at the scale $Q = m_t$.

Since a heavy top decays via $t \to bW$ in the standard model, the $pp \to t\bar{t}t\bar{t}$ mechanism is particularly interesting as a source of multiple W-boson production. Identification of W-bosons can be made via leptonic decays $W \to \ell\nu$ ($\ell = e, \mu$), though identification via hadronic jets may also be possible [9]. For $m_t = 140$ GeV, the preferred value from recent analyses of electroweak radiative corrections to M_W, M_Z and neutral current data [7], the cross section for producing $W^+W^+W^-W^-$ from the $t\bar{t}t\bar{t}$ source is about 0.5 pb (0.03 pb) at the SSC (LHC). For comparison, $q\bar{q} \to W^+W^+W^-W^-$ electroweak production [10] has a cross section of 6 fb (1 fb) at the SSC (LHC). The $t\bar{t}t\bar{t}$ production source of four W bosons will be accompanied by b jets from top quark decays and these jets will typically be hard with $p_T(b) \gtrsim 30$ GeV if $m_t \gtrsim 120$ GeV.

Table II shows the expected cross sections at the LHC and SSC for various four-W decay channels. To obtain event rates, we assume nominal annual integrated luminosity $\mathcal{L} = 10^4\,\text{pb}^{-1}$ for the SSC and $\mathcal{L} = 10^5\,\text{pb}^{-1}$ for the LHC, giving many thousands of four-W events per year. The branching fraction for all four W bosons to decay into $e\nu_e$ or $\mu\nu_\mu$ leptonic channels is $(0.216)^4 =$

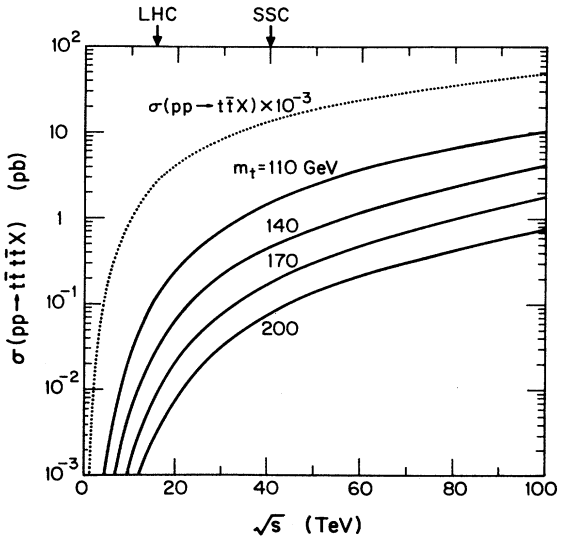

FIG. 5. Integrated cross sections for the production of two top quark pairs in pp collisions versus pp center-of-mass energy $\sqrt{s}$, for the cases $m_t = 110, 140, 170, 200$ GeV. LHC and SSC energies are indicated by arrows. The cross section for the production of a single top quark pair is shown for comparison, for the case $m_t = 140$ GeV.

TABLE II. Cross sections in fb for multiple W production from four top quarks at LHC and SSC; cross sections into different decay configurations are also shown (excluding $\tau\nu_\tau$ decays).

Source	LHC cross section (fb)		SSC cross section (fb)	
	$m_t = 110$ GeV	$m_t = 140$ GeV	$m_t = 110$ GeV	$m_t = 140$ GeV
$t\bar{t}t\bar{t} \to W^+W^+W^-W^-$	105	26	1500	460
four hadronic decays	22	5.4	310	96
one leptonic, three hadronic	28	6.9	400	120
two leptonic, two hadronic	13	3.3	190	60
three leptonic, one hadronic	2.9	0.71	41	13
four leptonic decays	0.23	0.057	3.3	1.0

2.22×10^{-3}, giving 10 (6) events per year at the SSC (LHC) from $4t$ production for $m_t = 140$ GeV. This is already at an interesting level. Higher branching fractions and event rates result for lower top mass or for channels with fewer W-decay leptons, as shown in Table II. Like-sign dilepton channels, obtained here from W^+W^+ or W^-W^- leptonic decays, have been proposed as clean signatures for supersymmetry [11]; however, the like-sign dilepton rate from four-top-quark production with $m_t = 110$–140 GeV, is comparable to that expected from pair production of gluinos with mass of 1 TeV.

To illustrate the character of four-top-quark events, we show a number of dynamical distributions at $\sqrt{s} = 40$ TeV for the m_t mass choices previously considered. Figure 6 gives the cross sections versus four-top-quark invariant mass $m_{t\bar{t}t\bar{t}}$; the distributions peak close above threshold but have high tails extending to very large invariant mass values, indicating that many of the four-top-quark SSC events will have summed hadronic energy $\sum E$ (excluding beam-pipe particles) of 2 TeV or more.

Experimentally, the summed transverse energy $\sum E_T$ of an event is another interesting quantity ($E_T = E \sin\theta$). The energy released in the decay of four top quarks with zero transverse momentum p_T would contribute on average approximately πm_t to $\sum E_T$; this contribution is increased when the top quarks have large p_T. Figure 7 gives the inclusive top-quark p_T distributions (summed over all t and $\bar{t}$); the curves peak near $p_T = m_t$ as may be expected on general grounds, and there are also substantial tails at higher p_T, indicating that not only large $\sum E$ but also large $\sum E_T$ may often be expected. It may sometimes be possible to identify individual t jets from their high invariant mass and their $t \to bW$ substructure; Fig. 7 shows that such jets will typically have quite high p_T.

Figure 8 gives the inclusive rapidity distributions of top quarks (summed over all t and $\bar{t}$), showing that they are predominantly produced in the central region. This result, however, does not guarantee that the decay products will pass into the central region of the detector. In a future paper, we will consider in more detail the final state decay products and subsequent detector signatures of four-top events.

Finally, it is interesting to comment on identical-

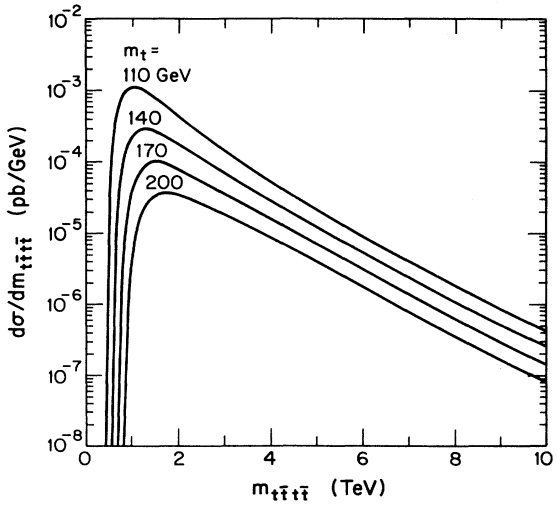

FIG. 6. Distributions versus the invariant mass of the four top quarks produced via $pp \to t\bar{t}t\bar{t}X$ at $\sqrt{s} = 40$ TeV, for several top quark masses.

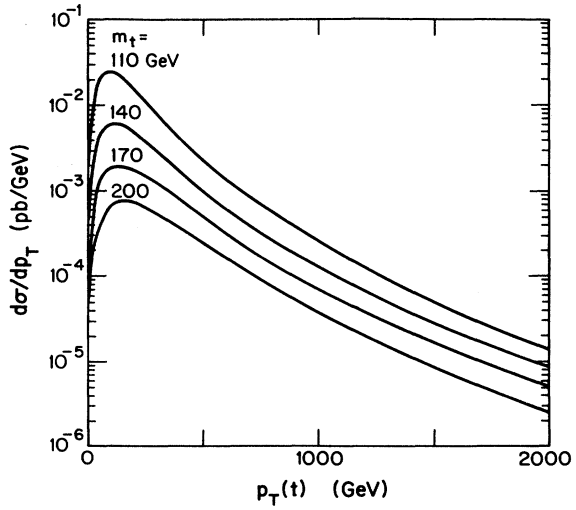

FIG. 7. Inclusive distributions versus the transverse momenta $p_T(t)$ of single t and $\bar{t}$ quarks at SSC energy $\sqrt{s} = 40$ TeV, for several top quark masses.

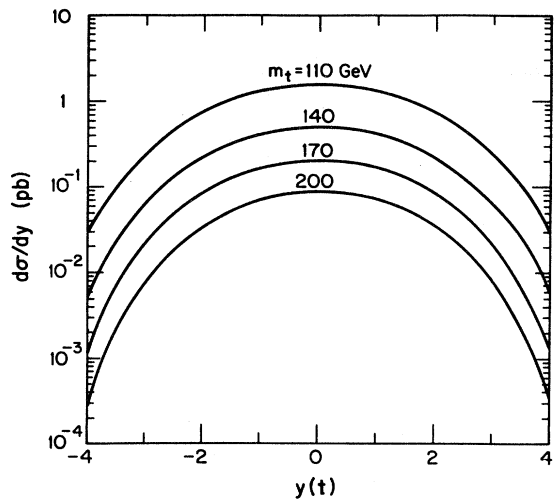

FIG. 8. Inclusive distributions versus the rapidities $y(t)$ of single t and $\bar{t}$ quarks at SSC energy $\sqrt{s} = 40$ TeV, for several top quark masses.

particle effects in our calculations. Comparing the production of two identical and two nonidentical quark pairs, with common mass m_Q, we find that the former case is suppressed relative to the latter by about a factor $\frac{1}{2}$ through the range of energies and masses considered here. This suppression factor appears to be primarily a combinatorial effect, analogous to the ratio $\frac{1}{2}$ between the production of massive lepton pairs in the $e^+e^-e^+e^-$ and $e^+e^-\mu^+\mu^-$ channels via virtual photons. In addition there may also be Pauli exclusion principle effects in some regions of phase space.

IV. SUMMARY

We have devised a new method for calculating the production of four heavy quarks at hadron colliders in lowest order QCD. Our method employs a numerical technique [1] to evaluate the color matrix and an amplitude level technique optimized for massive fermions using four component Dirac spinors. These techniques have been described in full.

To illustrate the interest of these processes, we have calculated the cross sections for $b\bar{b}b\bar{b}$, $b\bar{b}c\bar{c}$, and $c\bar{c}c\bar{c}$ production in $p\bar{p}$ collisions at $\sqrt{s} = 1.8$ TeV, corresponding to the Fermilab Tevatron energy. These channels offer new tests of QCD and also lead to multilepton events. Substantial cross sections are found; even when we require all four heavy quarks have transverse momenta $p_T > 10$ GeV, the cross sections exceed 100 pb at the Tevatron.

We have also calculated the production of four top quarks at pp supercollider energies. Such events will typically have large total energy and total transverse energy release. They will also contain four W bosons, assuming the standard $t \to bW$ decays. We have tabulated the predicted cross sections for various multi-W decay configurations at the LHC and SSC supercolliders at $\sqrt{s} = 15.4$ and 40 TeV, respectively. Even though the configurations where all four W bosons decay to $e\nu_e$ and $\mu\nu_\mu$ have a very small branching fraction, they may still be quite observable. With the nominal design luminosities, of order 10–30 all-leptonic four-W events may be expected per year at either the LHC or SSC, from four-top production with $m_t = 110$–140 GeV.

ACKNOWLEDGMENTS

We thank C. Goebel, T. Han, and W.-Y. Keung for discussions about identical particle effects. This research was supported in part by the University of Wisconsin Research Committee with funds granted by the Wisconsin Alumni Research Foundation, and in part by the U.S. Department of Energy under Contract No. DE-ACO2-76ER00881. Further support was provided by U.S. Department of Education Award No. P200A80214.

APPENDIX A

In this appendix we present the matrix elements and color matrix for the process

$$g^a(p_1)+g^b(p_2) \to Q_2^k(q_1)+\bar{Q}_2^l(q_2)+Q_3^m(q_3)+\bar{Q}_3^n(q_4) , \tag{A1}$$

where subscripts 2,3 denote quark flavors and superscripts $j,k,l,m = 1,2,3$ and $a,b = 1,\ldots,8$ label the color states; p_i and q_j denote the initial and final momenta. The p_i are incoming and the q_j are outgoing. There are 36 contributing Feynman diagrams some of which are shown in Fig. 1. However, due to the 4-gluon coupling in Fig. 1c, there are 38 distinct amplitudes.

To make it possible to compare to the results of others, we describe a method to obtain all Feynman diagrams from those in Fig. 1. To obtain an arbitrary Feynman diagram, say diagram r, look up row r in Table III. The second column in Table III gives a diagram letter corresponding to those in Fig. 1. The remaining four columns give the order in which the four final quark lines (labeled a,b,c,d in Fig. 1 and in the column headings) are assigned the momenta q_1, q_2, q_3, q_4.

To present the matrix elements we define

$$\begin{aligned} &q_1^2 = q_2^2 = m_{12}^2 , \quad q_3^2 = q_4^2 = m_{34}^2 , \\ &q_{12} = -q_1 - q_2 , \quad q_{34} = -q_3 - q_4 , \\ &p = p_1 + p_2, \quad j_1 = p_1 + q_{12}, \quad j_2 = p_1 + q_{34}. \end{aligned} \tag{A2}$$

The triple-gluon coupling is

$$\begin{aligned} \Gamma^\mu(q_1,q_2,\epsilon_1,\epsilon_2) = &-(2q_1+q_2)\cdot\epsilon_2\epsilon_1^\mu + (q_1-q_2)^\mu\epsilon_1\cdot\epsilon_2 \\ &+(2q_2+q_1)\cdot\epsilon_1\epsilon_2^\mu, \end{aligned} \tag{A3}$$

$$\bar{\Gamma}^\mu(p_1,p_2,\epsilon_1,\epsilon_2) = \Gamma^\mu(p_1,p_2,\epsilon_1,\epsilon_2)/(p_1+p_2)^2.$$

We define two quark currents

$$J^{\alpha}_{12} = \frac{\bar{u}(q_1)\gamma^{\alpha}v(q_2)}{(q_1+q_2)^2}\ , \quad J^{\alpha}_{34} = \frac{\bar{u}(q_3)\gamma^{\alpha}v(q_4)}{(q_3+q_4)^2}\ , \tag{A4}$$

where the γ^{α} are the Dirac gamma matrices. An often used quantity in the amplitudes is the coupling of an external gluon to an external quark leg. We can write this in a compact notation, including the effects of a corresponding quark propagator, as

$$\bar{u}_{ij} = \bar{u}(q_i)\ \not{\epsilon}_j \frac{(\not{q}_i - \not{p}_j + m_i)}{(q_i-p_j)^2 - m_i^2}, \tag{A5}$$

$$v_{ij} = \frac{(\not{p}_j - \not{q}_i + m_i)}{(p_j-q_i)^2 - m_i^2}\ \not{\epsilon}_j v(q_i),$$

where u, v are Dirac spinors. We denote the gluon polarization vectors by $\epsilon_1 = \epsilon(p_1)$ and $\epsilon_2 = \epsilon(p_2)$. Each amplitude must be multiplied by an overall coupling g_s^4 where $g_s = 4\pi\alpha_s$ is the QCD coupling. Using these definitions, the invariant amplitudes are

$$\mathcal{M}^1 = \Gamma^{\alpha}(p_2, q_{34}, \epsilon_2, J_{34})\bar{\Gamma}_{\alpha}(p_1, q_{12}, \epsilon_1, J_{12})\ , \tag{A6}$$
$$\mathcal{M}^2 = \bar{\Gamma}^{\alpha}(p_1, q_{34}, \epsilon_1, J_{34})\Gamma_{\alpha}(p_2, q_{12}, \epsilon_2, J_{12})\ , \tag{A7}$$
$$\mathcal{M}^3 = \bar{\Gamma}^{\alpha}(p_1, p_2, \epsilon_1, \epsilon_2)\Gamma_{\alpha}(q_{12}, q_{34}, J_{12}, J_{34})\ , \tag{A8}$$
$$\mathcal{M}^4 = J^{\alpha}_{12}J^{\beta}_{34}(\epsilon_{1\beta}\epsilon_{2\alpha} - \epsilon_1\cdot\epsilon_2 g_{\alpha\beta})\ , \tag{A9}$$
$$\mathcal{M}^5 = J^{\alpha}_{12}J^{\beta}_{34}(\epsilon_1\cdot\epsilon_2 g_{\alpha\beta} - \epsilon_{1\alpha}\epsilon_{2\beta})\ , \tag{A10}$$
$$\mathcal{M}^6 = J^{\alpha}_{12}J^{\beta}_{34}(\epsilon_{1\alpha}\epsilon_{2\beta} - \epsilon_{1\beta}\epsilon_{2\alpha})\ , \tag{A11}$$
$$\mathcal{M}^7 = \bar{u}_{11}\ \bar{\not{\epsilon}}(p_2, q_{34}, \epsilon_2, J_{34})v(q_2)\ , \tag{A12}$$
$$\mathcal{M}^8 = \bar{u}(q_1)\ \bar{\not{\epsilon}}(p_2, q_{34}, \epsilon_2, J_{34})v_{21}\ , \tag{A13}$$
$$\mathcal{M}^9 = \bar{u}_{31}\ \bar{\not{\epsilon}}(p_2, q_{12}, \epsilon_2, J_{12})v(q_4)\ , \tag{A14}$$
$$\mathcal{M}^{10} = \bar{u}(q_3)\ \bar{\not{\epsilon}}(p_2, q_{12}, \epsilon_2, J_{12})v_{41}\ , \tag{A15}$$
$$\mathcal{M}^{11} = \bar{u}(q_3)\ \bar{\not{\epsilon}}(p_1, q_{12}, \epsilon_1, J_{12})v_{42}\ , \tag{A16}$$
$$\mathcal{M}^{12} = \bar{u}_{32}\ \bar{\not{\epsilon}}(p_1, q_{12}, \epsilon_1, J_{12})v(q_4)\ , \tag{A17}$$
$$\mathcal{M}^{13} = \bar{u}(q_1)\ \bar{\not{\epsilon}}(p_1, q_{34}, \epsilon_1, J_{34})v_{22}\ , \tag{A18}$$
$$\mathcal{M}^{14} = \bar{u}_{12}\ \bar{\not{\epsilon}}(p_1, q_{34}, \epsilon_1, J_{34})v(q_4)\ , \tag{A19}$$
$$\mathcal{M}^{15} = \bar{u}_{11}\gamma^{\alpha}v(q_2)\bar{u}(q_3)\gamma_{\alpha}v_{42}/j_1^2\ , \tag{A20}$$
$$\mathcal{M}^{16} = \bar{u}(q_1)\gamma^{\alpha}v_{21}\bar{u}(q_3)\gamma_{\alpha}v_{42}/j_1^2\ , \tag{A21}$$
$$\mathcal{M}^{17} = \bar{u}_{11}\gamma^{\alpha}v(q_4)\bar{u}_{32}\gamma_{\alpha}v(q_4)/j_1^2\ , \tag{A22}$$
$$\mathcal{M}^{18} = \bar{u}(q_1)\gamma^{\alpha}v_{21}\bar{u}_{32}\gamma_{\alpha}v(q_4)/j_1^2\ , \tag{A23}$$
$$\mathcal{M}^{19} = \bar{u}_{31}\gamma^{\alpha}v(q_4)\bar{u}(q_1)\gamma_{\alpha}v_{22}/j_2^2\ , \tag{A24}$$

TABLE III. Feynman diagram permutations.

Diagram	Letter	a	b	c	d
1	a	1	2	3	4
2	a	3	4	1	2
3	b	1	2	3	4
4	c	1	2	3	4
5	c	1	2	3	4
6	c	1	2	3	4
7	d	1	2	3	4
8	d	2	1	3	4
9	d	3	4	1	2
10	d	4	3	1	2
11	e	1	2	3	4
12	e	1	2	4	3
13	e	3	4	1	2
14	e	3	4	2	1
15	f	1	2	3	4
16	f	2	1	3	4
17	f	1	2	4	3
18	f	2	1	4	3
19	f	3	4	1	2
20	f	4	3	1	2
21	f	3	4	2	1
22	f	4	3	2	1
23	g	1	3	4	2
24	h	1	3	4	2
25	i	1	3	4	2
26	i	2	3	4	1
27	h	2	3	4	1
28	g	2	3	4	1
29	g	3	1	2	4
30	h	3	1	2	4
31	i	3	1	2	4
32	i	4	1	2	3
33	h	4	1	2	3
34	g	4	1	2	3
35	j	1	3	4	2
36	k	1	3	4	2
37	j	3	1	2	4
38	k	3	1	2	4

$$\mathcal{M}^{20} = \bar{u}(q_3)\gamma^{\alpha}v_{41}\bar{u}(q_1)\gamma_{\alpha}v_{22}/j_2^2\ , \tag{A25}$$
$$\mathcal{M}^{21} = \bar{u}_{31}\gamma^{\alpha}v(q_4)\bar{u}_{12}\gamma_{\alpha}v(q_2)/j_2^2\ , \tag{A26}$$
$$\mathcal{M}^{22} = \bar{u}(q_3)\gamma^{\alpha}v_{41}\bar{u}_{32}\gamma_{\alpha}v(q_2)/j_2^2\ . \tag{A27}$$

For the following diagrams, we define

$$\begin{aligned}
\bar{u}_{1,34} &= \bar{u}(q_1)\ \not{J}_{34}(\not{q}_1 - \not{q}_{34} + m_{12})/[(q_1-q_{34})^2 - m_{12}^2 + im_{12}\Gamma_{12}]\ ,\\
\bar{u}_{3,12} &= \bar{u}(q_3)\ \not{J}_{12}(\not{q}_3 - \not{q}_{12} + m_{34})/[(q_3-q_{12})^2 - m_{34}^2 + im_{34}\Gamma_{34}]\ ,\\
v_{2,34} &= (\not{q}_{34} - \not{q}_2 + m_{12})\ \not{J}_{34}v(q_2)/[(q_{34}-q_2)^2 - m_{12}^2 + im_{12}\Gamma_{12}]\ ,\\
v_{4,12} &= (\not{q}_{12} - \not{q}_4 + m_{34})\ \not{J}_{12}v(q_4)/[(q_{12}-q_4)^2 - m_{34}^2 + im_{34}\Gamma_{34}]\ ,
\end{aligned} \tag{A28}$$

where Γ_{12} and Γ_{34} are the top-quark decay widths.

$$\mathcal{M}^{23} = \bar{u}_{1,34}\, \not{\epsilon}_1 v_{22} \,, \tag{A29}$$

$$\mathcal{M}^{24} = \bar{u}_{11}\, \not{J}_{34} v_{22} \,, \tag{A30}$$

$$\mathcal{M}^{25} = \bar{u}_{11}\, \not{\epsilon}_2 v_{2,34} \,, \tag{A31}$$

$$\mathcal{M}^{26} = \bar{u}_{1,34}\, \not{\epsilon}_2 v_{21} \,, \tag{A32}$$

$$\mathcal{M}^{27} = \bar{u}_{12}\, \not{J}_{34} v_{21} \,, \tag{A33}$$

$$\mathcal{M}^{28} = \bar{u}_{12}\, \not{\epsilon}_1 v_{2,34} \,, \tag{A34}$$

$$\mathcal{M}^{29} = \bar{u}_{3,12}\, \not{\epsilon}_1 v_{42} \,, \tag{A35}$$

$$\mathcal{M}^{30} = \bar{u}_{31}\, \not{J}_{34} v_{42} \,, \tag{A36}$$

$$\mathcal{M}^{31} = \bar{u}_{31}\, \not{\epsilon}_2 v_{4,12} \,, \tag{A37}$$

$$\mathcal{M}^{32} = \bar{u}_{3,12}\, \not{\epsilon}_2 v_{41} \,, \tag{A38}$$

TABLE IV. Eigenvalues for $gg \to q\bar{q}q'\bar{q}'$.

Eigenvalue	
a	96.990 118
b	92.952 845
c	27
d	30.908 051
e	12.5
f	7.594 251 1
g	1.102 709 6
h	2.5
i	1.637 852 9
j	1.091 948 4
k	5/6

TABLE V. Normalized eigenvectors for the color matrix of $gg \to q\bar{q}q'\bar{q}'$; the values of the components a_i, b_i, etc. are listed in Table VI.

Diagram number	Eigenvalue										
	a	b	c	d	e	f	g	h	i	j	k
1	$2a_1$	$2b_1$				$-2f_1$	$-2g_1$		$2i_1$		
2	$2a_1$	$-2b_1$				$-2f_1$	$2g_1$		$2i_1$		
3		$4b_1$					$-4g_1$				
4	$2a_1$	$-2b_1$				$2f_1$	$2g_1$		$-2i_1$		
5	$2a_1$	$-2b_1$				$-2f_1$	$2g_1$		$2i_1$		
6		$4b_1$					$-4g_1$				
7	$-a_1$	$-b_1$	$7c_1$	d_1	$-e_1$	f_1	g_1		$-2i_1$	$-j_1$	
8	a_1	b_1	$7c_1$	d_1	$-e_1$	$-f_1$	$-g_1$		i_1	$-j_1$	
9	$-a_1$	b_1	$-7c_1$	d_1	e_1	f_1	$-g_1$		$-i_1$	$-j_1$	
10	a_1	$-b_1$	$-7c_1$	d_1	e_1	$-f_1$	g_1		i_1	$-j_1$	
11	a_1	b_1	$7c_1$	$-d_1$	e_1	$-f_1$	$-g_1$		i_1	j_1	
12	$-a_1$	$-b_1$	$7c_1$	$-d_1$	e_1	f_1	g_1		$-i_1$	j_1	
13	a_1	$-b_1$	$-7c_1$	$-d_1$	$-e_1$	$-f_1$	g_1		i_1	j_1	
14	$-a_1$	b_1	$-7c_1$	$-d_1$	$-e_1$	f_1	$-g_1$		$-i_1$	j_1	
15	a_2	$-b_2$		d_1	$-e_1$	f_2	$-g_2$		$-i_2$	$-j_1$	
16	a_3	b_3	$7c_1$			f_3	$-g_3$		$-i_3$		
17	a_3	b_3	$-7c_1$			f_3	$-g_3$		$-i_3$		
18	a_2	$-b_2$		$-d_1$	e_1	f_2	$-g_2$		$-i_2$	j_1	
19	a_2	b_2		d_1	e_1	f_2	g_2		$-i_2$	$-j_1$	
20	a_3	$-b_3$	$-7c_1$			f_3	g_3		$-i_3$		
21	a_3	$-b_3$	$7c_1$			f_3	g_3		$-i_3$		
22	a_2	b_2		$-d_1$	$-e_1$	f_2	g_2		$-i_2$	j_1	
23	a_4	b_1	c_1	d_2	e_1	f_4	$-g_1$	h_1	i_4	j_2	$-k_1$
24	a_5		$-6c_1$	$-d_3$		f_5		h_1	i_5	j_3	$-k_1$
25	a_4	$-b_1$	c_1	d_2	$-e_1$	f_4	g_1	h_1	i_4	j_2	$-k_1$
26	a_4	$-b_1$	$-c_1$	$-d_2$	e_1	f_4	g_1	$-h_1$	i_4	$-j_2$	$-k_1$
27	a_5		$6c_1$	d_3		f_5		$-h_1$	i_5	$-j_3$	$-k_1$
28	a_4	b_1	$-c_1$	$-d_2$	$-e_1$	f_4	$-g_1$	$-h_1$	i_4	$-j_2$	$-k_1$
29	a_4	$-b_1$	$-c_1$	d_2	$-e_1$	f_4	g_1	$-h_1$	i_4	j_2	k_1
30	a_5		$6c_1$	$-d_3$		f_5		$-h_1$	i_5	j_3	k_1
31	a_4	b_1	$-c_1$	d_2	e_1	f_4	$-g_1$	$-h_1$	i_4	j_2	k_1
32	a_4	b_1	c_1	$-d_2$	$-e_1$	f_4	$-g_1$	h_1	i_4	$-j_2$	k_1
33	a_5		$-6c_1$	d_3		f_5		h_1	i_5	$-j_3$	k_1
34	a_4	$-b_1$	c_1	$-d_2$	e_1	f_4	g_1	h_1	i_5	$-j_2$	k_1
35		$2b_1$	$2c_1$	$2d_2$			$-2g_1$	$2h_1$		$2j_2$	
36		$-2b_1$	$2c_1$	$2d_2$			$2g_1$	$2h_1$		$2j_2$	
37		$-2b_1$	$-2c_1$	$2d_2$			$2g_1$	$-2h_1$		$2j_2$	
38		$2b_1$	$-2c_1$	$2d_2$			$-2g_1$	$-2h_1$		$2j_2$	

TABLE VI. Eigenvector component values.

Eigenvalue	Subscript				
	1	2	3	4	5
a	0.186 531	$-7.534\,99 \times 10^{-2}$	0.111 181	$-6.174\,04 \times 10^{-2}$	0.124 719
b	0.110 008	$2.407\,65 \times 10^{-2}$	$8.593\,16 \times 10^{-2}$		
c	$1/\sqrt{756}$				
d	0.188 803	0.154 265	$3.377\,08 \times 10^{-2}$		
e	$1/\sqrt{20}$				
f	$5.383\,18 \times 10^{-3}$	0.194 668	0.189 285	0.244 06	0.238 679
g	$9.660\,13 \times 10^{-3}$	0.347 368	0.357 028		
h	$1/\sqrt{28}$				
i	$7.789\,51 \times 10^{-3}$	0.300 245	0.292 456	0.154 372	0.162 161
j	0.171 631	0.286 693	0.115 062		
k	$1/\sqrt{12}$				

$$\mathcal{M}^{33} = \bar{u}_{32}\, \not{J}_{12} v_{41} \,, \tag{A39}$$
$$\mathcal{M}^{34} = \bar{u}_{32}\, \not{\epsilon}_1 v_{4,12} \,, \tag{A40}$$
$$\mathcal{M}^{35} = \bar{u}_{1,34}\, \bar{\not{Y}}(p_1,p_2,\epsilon_1,\epsilon_2) v(q_2) \,, \tag{A41}$$
$$\mathcal{M}^{36} = \bar{u}(q_1)\, \bar{\not{Y}}(p_1,p_2,\epsilon_1,\epsilon_2) v_{2,34} \,, \tag{A42}$$
$$\mathcal{M}^{37} = \bar{u}_{3,12}\, \bar{\not{Y}}(p_1,p_2,\epsilon_1,\epsilon_2) v(q_4) \,, \tag{A43}$$
$$\mathcal{M}^{38} = \bar{u}(q_3)\, \bar{\not{Y}}(p_1,p_2,\epsilon_1,\epsilon_2) v_{4,12} \,. \tag{A44}$$

There are eleven nonzero eigenvalues in the color matrix for $gg \to q\bar{q}q'\bar{q}'$ where the quarks are nonidentical. The nonzero eigenvalues are presented in Table IV with the corresponding normalized eigenvectors presented in Table V and Table VI. Where possible we have deduced rational expressions for the eigenvalues and eigenvectors, otherwise we have presented the numerical results.

APPENDIX B

In this appendix we present the matrix elements for the process

$$q_1^i(p_1) + \bar{q}_1^j(p_2) \to Q_2^k(q_1) + \bar{Q}_2^l(q_2) + Q_3^m(q_3) + \bar{Q}_3^n(q_4) \,, \tag{B1}$$

where the subscripts $1,2,3$ denote quark flavors, superscripts i,j,k,l,m,n label the color states, and p_1, p_2 and q_1, q_2, q_3, q_4 are the external momenta; p_i are incoming and q_i are outgoing.

For each of the seven contributing diagrams, shown in Fig. 2, we present the invariant amplitudes and the eigenvalues and eigenvectors of the corresponding color matrix. The amplitudes are labeled to correspond to the diagrams in Fig. 2.

In addition to the quantities defined in Appendix A we define

$$P^\mu = \frac{\bar{v}(p_2)\gamma^\mu u(p_1)}{(p_1+p_2)^2} \,. \tag{B2}$$

Using this definition, the amplitudes are

$$\mathcal{M}^a = \bar{v}(p_2)\, \not{J}_{34}\, \not{J}_1\, \not{J}_{12} u(p_1)/j_1^2 \,, \tag{B3}$$
$$\mathcal{M}^b = \bar{v}(p_2)\, \not{J}_{12}\, \not{J}_2\, \not{J}_{34} u(p_1)/j_2^2 \,, \tag{B4}$$
$$\mathcal{M}^c = P_\alpha \Gamma^\alpha(q_{12}, q_{34}, J_{12}, J_{34}) \,, \tag{B5}$$
$$\mathcal{M}^d = \bar{u}_{1,34}\, \not{P} v(q_2) \,, \tag{B6}$$
$$\mathcal{M}^e = \bar{u}(q_1)\, \not{P} v_{2,34} \,, \tag{B7}$$
$$\mathcal{M}^f = \bar{u}_{3,12}\, \not{P} v(q_4) \,, \tag{B8}$$
$$\mathcal{M}^g = \bar{u}(q_3)\, \not{P} v_{4,12} \,. \tag{B9}$$

There are four nonzero eigenvalues in the color matrix for this process. These eigenvalues and the corresponding eigenvectors are

$$\lambda_1 = \frac{1}{3}, \quad \hat{\lambda}_1 = \frac{1}{\sqrt{28}}(2,\ 2,\ 0,-3,-3,\ 1,\ 1)^T \,;$$
$$\lambda_2 = \frac{15}{2} \,, \quad \hat{\lambda}_2 = \frac{1}{\sqrt{10}}(-1,\ 1,\ 2,\ 1,\ -1,-1,\ 1)^T \,;$$
$$\lambda_3 = \frac{17}{6} \,, \quad \hat{\lambda}_3 = \frac{1}{\sqrt{6}}(1,\ 1,\ 0,\ 1,\ 1,\ 1,\ 1)^T \,; \tag{B10}$$
$$\lambda_4 = \frac{1}{3} \,, \quad \hat{\lambda}_4 = \frac{1}{\sqrt{84}}(-4,-4,\ 0,-1,-1,\ 5,\ 5)^T \,,$$

where T stands for the transpose and the rational fractions shown for the eigenvalues are inferred (up to double precision accuracy).

[1] V. Barger, R. J. N. Phillips, and A. L. Stange, University of Wisconsin at Madison Report No. MAD/PH/621, 1991 (unpublished).

[2] J. F. Gunion and Z. Kunszt, Phys. Lett. **159B**, 167 (1985); Phys. Lett. B **176**, 477 (1986).

[3] F. A. Berends, R. Kleiss, P. de Causmaecker, R. Gastmans, and T. T. Wu, Phys. Lett. **103B**, 124 (1981); P. de Causmaecker, R. Gastmans, W. Troost, and T. T. Wu, Nucl. Phys. **B206**, 53 (1982); F. A. Berends, P. de Causmaecker, R. Gastmans, and T. T. Wu, *ibid.* **B206**, 61 (1982); D. Zeppenfeld, Int. J. Mod. Phys. A **3**, 2175 (1988); K. Hagiwara and D. Zeppenfeld, Nucl. Phys. **B313**, 560 (1989).

[4] H. Baer, V. Barger, H. Goldberg, and R. J. N. Phillips,

Phys. Rev. D **37**, 3152 (1988); R. S. Fletcher, F. Halzen, and C. S. Kim, Phys. Lett. B **209**, 351, (1988); H. Baer, V. Barger, H. Goldberg, and J. Ohnemus, Phys. Rev. D **38**, 3467 (1988).

[5] P. N. Harriman, A. D. Martin, W. J. Stirling, and R. G. Roberts, Phys. Rev. D **42**, 798 (1990); we use solution B, usually denoted HMRSB.

[6] Collider Detector at Fermilab Collaboration, report by G. P. Yeh to La Thuile Conference, 1990 (unpublished).

[7] U. Amaldi *et al.*, Phys. Rev. D **36**, 1385 (1985); G. Costa *et al.*, Nucl. Phys. **B297**, 244 (1988); P. Langacker, Phys. Rev. Lett. **63**, 1920, (1989); V. Barger, J. L. Hewett, and T. G. Rizzo, *ibid.* **65**, 1313 (1990); J. Ellis and G. F. Fogli, Phys Lett. B **249**, 543, (1990); F. Halzen and B. Kniehl, Nucl. Phys. **B353**, 567 (1991); F. Halzen and D. A. Morris, Phys. Lett. B **237**, 107, (1990); T. G. Rizzo, University of Wisconsin at Madison Report No. MAD/PH/608, 1990 (unpublished).

[8] Z. Kunszt, Nucl. Phys. **B247**, 339 (1984); Z. Kunszt and W. J. Stirling, Phys. Lett. B **171**, 307 (1986).

[9] UA2 Collaboration, J. Alitti *et al.*, Z. Phys C **49**, 17 (1991); G. L. Kane and C. P. Yuan, Phys. Rev. D **40**, 2231, (1989).

[10] V. Barger, T. Han, and H. Pi, Phys. Rev. D **41**, 824 (1990).

[11] H. Baer *et al.*, in *Proceedings of the 1990 DPF Summer Study on High Energy Physics*, Snowmass, Colorado, edited by E. L. Berger and J. Butler (World Scientific, Singapore, in press).